

## RESEARCH ARTICLE SUMMARY

## ASTEROIDS

## Widespread carbon-bearing materials on near-Earth asteroid (101955) Bennu

Amy A. Simon\*, Hannah H. Kaplan, Victoria E. Hamilton, Dante S. Lauretta, Humberto Campins, Joshua P. Emery, M. Antonietta Barucci, Daniella N. DellaGiustina, Dennis C. Reuter, Scott A. Sandford, Dathon R. Golish, Lucy F. Lim, Andrew Ryan, Benjamin Rozitis, Carina A. Bennett

**INTRODUCTION:** Owing to their low reflectance and spectral similarity to primitive carbonaceous chondrite meteorites, C-complex asteroids are thought to contain carbon-bearing material. The OSIRIS-REx (Origins, Spectral Interpretation, Resource Identification, and Security-Regolith Explorer) spacecraft is designed to return a sample of carbonaceous material from the near-Earth C-complex asteroid (101955) Bennu. The selection of a suitable sample site necessitated global mapping and characterization of Bennu's surface. Spatially resolved spectral mapping can determine the surface properties and composition of Bennu. It also provides context for both the sample that will be returned and the interpretation of unresolved observations of other dark asteroids.

**RATIONALE:** We used data acquired by the OSIRIS-REx Visible and InfraRed Spectrometer (OVIRS), a point spectrometer that covers the wavelength range from 0.4 to 4.3  $\mu\text{m}$ , to map the physical and compositional characteristics of Bennu's surface. These data allow us to search for spectral signatures of carbon bearing materials on Bennu. The 3.4- $\mu\text{m}$  region is sensitive to carbonate or organic materials, which produce absorption bands at this wavelength because of either  $\text{CO}_3^{2-}$  stretching and

vibration or C-H stretching. OVIRS mapping provided global coverage of Bennu at  $\sim 600\text{-m}^2$  areal resolution at several local solar times. Using the data with the highest solar illumination ( $\sim 9^\circ$  phase, 12:30 p.m. local solar time), we mapped the depth of the 3.4- $\mu\text{m}$  absorption band, peak temperature, 0.55- $\mu\text{m}$  brightness, spectral slope from 0.5 to 1.5  $\mu\text{m}$ , and the distribution of the 2.74- $\mu\text{m}$  absorption band of hydrated minerals, which was previously detected in unresolved observations.

**RESULTS:** The 3.4- $\mu\text{m}$  absorption band, indicative of carbon-bearing materials, is detected over all of Bennu's surface with band depths of a few percent. The band shape varies with surface location and spans the range of 3.4- $\mu\text{m}$  band shapes seen on other dark C-complex asteroids. The differing band shapes persist at higher areal resolution ( $60\text{ m}^2$ ) and at several phase angles. The spectra collected at  $60\text{ m}^2$  show that the deepest bands occur over distinct boulders.

The distribution of the 3.4- $\mu\text{m}$  band on Bennu's surface does not correlate with the distributions of temperature, brightness, spectral slope, or the 2.74- $\mu\text{m}$  absorption band, although some of these features correlate weakly with each other. At low phase angles, the darkest areas ( $\sim 3\%$  reflectance at 0.55  $\mu\text{m}$ ) are correlated

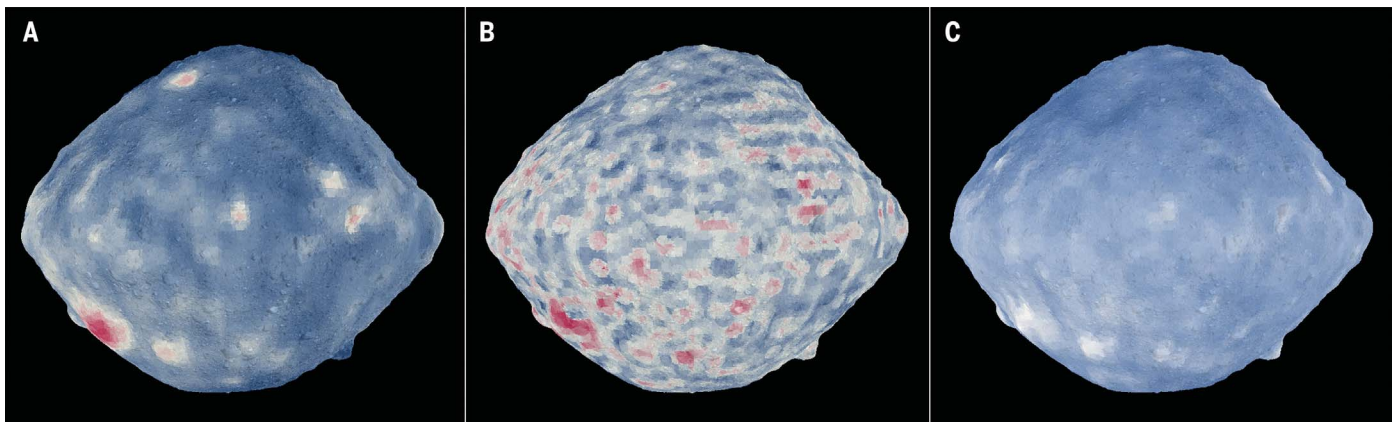
with the hottest surface temperatures ( $\sim 350\text{ K}$ ), with a Spearman's rank correlation coefficient,  $r$ , of 0.65.

The absorption feature at 2.74  $\mu\text{m}$ , indicative of hydrated phyllosilicates, is globally present, with band depths of 12 to 17% that correlate with surface temperature and latitude ( $|r| = 0.76$  and  $0.58$ , respectively). When the temperature trend is removed, the correlation of hydrated phyllosilicates with latitude is weaker ( $|r| = 0.48$ ). In OVIRS data, Bennu's global surface has an overall blue (negative) spectral slope from 0.5 to 1.5  $\mu\text{m}$ , with some boulders and craters that are redder (less negative) than average, consistent with results from multispectral imaging. Some of the darkest material is spectrally blue, whereas some is spectrally red, indicating local differences in composition, space weathering, and/or particle size.

**CONCLUSION:** The variation in the shape of the 3.4- $\mu\text{m}$  band indicates a mix of organics and carbonates on Bennu's surface, likely inherited from the collisional disruption of its parent asteroid. To retain a widespread 3.4- $\mu\text{m}$  organic feature, most of the material on Bennu's surface could not have been exposed to the space environment for more than a few million years. The samples returned to Earth by the OSIRIS-REx spacecraft should contain ample amounts of these materials, regardless of sampling location. Variable 3.4- $\mu\text{m}$  band depths over individual boulders may be due to compositional differences or to exposure of fresh material by means of thermally driven fracturing. ■

The list of author affiliations is available in the full article online.  
\*Corresponding author. Email: amy.simon@nasa.gov  
Cite this article as A. A. Simon et al., *Science* **370**, eabc3522 (2020). DOI: 10.1126/science.abc3522

**S** READ THE FULL ARTICLE AT  
<https://doi.org/10.1126/science.abc3522>



**Spectral variations on Bennu's 60°E hemisphere.** (A) Visible to near-infrared (0.5 to 1.5  $\mu\text{m}$ ) slope. Blue denotes more steeply negative slopes (decreasing brightness with increasing wavelength); red denotes shallower slopes. (B) Band area at 3.4  $\mu\text{m}$ , indicative of carbon-bearing materials. Blue indicates smaller band areas; red, larger band areas. (C) Band depth at 2.74  $\mu\text{m}$ , indicative of hydrated phyllosilicates. White indicates shallower bands; blue, deeper bands.

## RESEARCH ARTICLE

## ASTEROIDS

## Widespread carbon-bearing materials on near-Earth asteroid (101955) Bennu

Amy A. Simon<sup>1\*</sup>, Hannah H. Kaplan<sup>2</sup>, Victoria E. Hamilton<sup>2</sup>, Dante S. Lauretta<sup>3</sup>, Humberto Campins<sup>4</sup>, Joshua P. Emery<sup>5</sup>, M. Antonietta Barucci<sup>6</sup>, Daniella N. DellaGiustina<sup>3</sup>, Dennis C. Reuter<sup>1</sup>, Scott A. Sandford<sup>7</sup>, Dathon R. Golish<sup>3</sup>, Lucy F. Lim<sup>1</sup>, Andrew Ryan<sup>3</sup>, Benjamin Rozitis<sup>8</sup>, Carina A. Bennett<sup>3</sup>

Asteroid (101955) Bennu is a dark asteroid on an Earth-crossing orbit that is thought to have assembled from the fragments of an ancient collision. We use spatially resolved visible and near-infrared spectra of Bennu to investigate its surface properties and composition. In addition to a hydrated phyllosilicate band, we detect a ubiquitous 3.4-micrometer absorption feature, which we attribute to a mix of organic and carbonate materials. The shape and depth of this absorption feature vary across Bennu's surface, spanning the range seen among similar main-belt asteroids. The distribution of the absorption feature does not correlate with temperature, reflectance, spectral slope, or hydrated minerals, although some of those characteristics correlate with each other. The deepest 3.4-micrometer absorptions occur on individual boulders. The variations may be due to differences in abundance, recent exposure, or space weathering.

**A**steroid (101955) Bennu is a dark near-Earth asteroid averaging 4.4% reflectance (1), thought to be a collisional remnant of a much larger object in the main asteroid belt (2). Bennu is classified as a C-complex asteroid—a body with low reflectance and spectral similarities to carbonaceous chondrite meteorites—so is expected to have high carbon content (3). Specifically, Bennu belongs to a subgroup of the C-complex, the B-types, which have bluer spectra (4) and are thought to have silicates, hydrated minerals, organic molecules, magnetite, and sulfides on their surfaces (5).

Launched in 2016, the OSIRIS-REx (Origins, Spectral Interpretation, Resource Identification, and Security—Regolith Explorer) spacecraft is designed to return a sample of carbonaceous material from Bennu to Earth for laboratory analysis (6). One of the mission objectives is to compare ground-based Bennu data with the resolved surface to help interpret unresolved observations of other asteroids (6). Detailed spatial and spectral maps will also be required to tie the returned sample to its local geologic context.

The B-type asteroids are subdivided according to their visible to near-infrared (VIS-NIR)

spectral slopes, with some bluer objects similar to (2) Pallas, some redder objects similar to (24) Themis, and others in the continuum of spectral slopes between them (7). Each of these VIS-NIR spectral slopes can be matched with analogous carbonaceous chondrite meteorites, which show various degrees of aqueous and thermal alteration (5). On the basis of these meteorite comparisons, it has been proposed that the redder-sloped B-types are the most water-rich, similar to the CM class of chondrites, and the bluer-sloped B-types are dry and have been heated or thermally metamorphosed, similar to the CK4 class of chondrites (5). Before the OSIRIS-REx spacecraft's arrival, one of the closest spectral matches to Bennu's blue spectral slope (at <1.5 μm) was a carbonaceous chondrite that shows signs of having been aqueously altered then heated and dehydrated (8). However, global spectra acquired during the spacecraft's approach to Bennu showed a 2.7-μm absorption band, indicating hydrated minerals, with a shape more similar to that of the aqueously altered CM chondrites (9).

Bennu is thought to be a member of either the (142) Polana or the (495) Eulalia collisional family, groups of asteroids that appear to originate from a common source in the main asteroid belt between Mars and Jupiter (10, 11). Both Polana and Eulalia reside in the main belt and have spectra that indicate that they are members of the C-complex (12). The Hayabusa2 spacecraft has visited and sampled the near-Earth asteroid (162173) Ryugu, which is also likely to be a member of the Polana or Eulalia family, but is classified as a near-Earth Cb-type asteroid, a different spectral subgroup of the C-complex (13). Spatially resolved spectra from

Hayabusa2 indicate that Ryugu has a weaker global 2.7-μm hydration feature than Bennu. On Ryugu, the band varies only slightly (7 to 10% band depth) across the surface, which is consistent with thermal processing (14). Other asteroid families, such as the (24) Themis family, show spectral diversity among their members and evidence of material separation, possibly into rock and ice—likely enough to produce aqueous alteration (15). Similar processing may have occurred in the parent body of Bennu. Bennu is a rubble-pile asteroid, an agglomeration of collision fragments, that was ejected from the main asteroid belt and migrated to its final near-Earth orbit. Global maps of Bennu's spectral characteristics are required to understand its relationship to Ryugu and their parent population and to the broader classes of B- and C-type asteroids.

In 2019, the OSIRIS-REx mission completed a campaign of close-proximity observation of Bennu to determine suitable sites for sample collection, which occurred 20 October 2020 (6). The OSIRIS-REx Visible and InfraRed Spectrometer (OVIRS) acquired global surface data from 0.4 to 4.3 μm at multiple phase angles (16). Visible wavelengths are used to determine the overall color variations across Bennu's surface and its mineral content, whereas the NIR is sensitive to surface temperature and compositional variations. The OVIRS NIR coverage around 2.7 μm has been used to detect the global presence of hydrated minerals (9), and the region from 3.2 to 3.6 μm is sensitive to carbonate (CO<sub>3</sub><sup>2-</sup> stretching or vibration) and organic (C-H stretching) absorption bands.

In this study, we investigated the spectrum of Bennu using OVIRS observations and searched for evidence of absorption bands attributable to carbon-bearing materials. Our goal was to compare the shape of any carbon-bearing absorption features with spectra of other C-complex asteroids and determine the surface distribution of carbon-bearing materials.

## Observations and mapping

We used data from the Equatorial Stations subphase (25 April to 6 June 2019) of the OSIRIS-REx Detailed Survey phase, which ran from 7 March through 6 June 2019. The subphase was composed of data collection from seven spacecraft stations, each positioned close to the equator at a different local solar time and ~5 km above the surface (6). As OVIRS is a point spectrometer, with a circular 4-mrad field of view, each spectrum covers all wavelengths simultaneously for a spot on the surface (16). At each local solar time, the spacecraft nodded along lines of constant longitude at ~2 mrad s<sup>-1</sup> to achieve nearly global OVIRS coverage as the asteroid rotated below. Although OVIRS observed most latitudes and longitudes at each station, the individual spots were not

<sup>1</sup>Solar System Exploration Division, NASA Goddard Space Flight Center, Greenbelt, MD, USA. <sup>2</sup>Southwest Research Institute, Boulder, CO, USA. <sup>3</sup>Lunar and Planetary Laboratory, University of Arizona, Tucson, AZ, USA. <sup>4</sup>Department of Physics, University of Central Florida, Orlando, FL, USA.

<sup>5</sup>Department of Astronomy and Planetary Sciences, Northern Arizona University, Flagstaff, AZ, USA. <sup>6</sup>Laboratoire d'Etudes Spatiales et d'Instrumentation en Astrophysique, Observatoire de Paris, Université Paris Sciences et Lettres, Centre National de la Recherche Scientifique, Université de Paris, Sorbonne Université, Meudon, France. <sup>7</sup>NASA Ames Research Center, Moffett Field, CA, USA. <sup>8</sup>School of Physical Sciences, The Open University, Milton Keynes, UK.

\*Corresponding author. Email: amy.simon@nasa.gov

centered at the exact same locations from station to station. The spot spatial resolution was  $\sim 20$  m cross-track and 30 m along-track at the equator. Surface projection increases the along-track spot size at higher latitudes, and local surface slopes also cause the resolution to vary. From these data, we produced global OVIRS maps at  $\sim 600\text{-m}^2$  equatorial areal resolution from the stations at 10:00 a.m., 12:30 p.m., and 3:00 p.m. local solar time, as these have the highest available solar illumination and maximum surface temperatures.

From 4 to 27 October 2019, the spacecraft conducted lower-altitude reconnaissance flyovers of four candidate sample sites and surrounding context regions, scanning each area of interest at a range of 1 to 1.3 km (6). Reconnaissance flyovers occurred when Benu was at a greater distance from the Sun than during the Detailed Survey, and therefore solar illumination was lower; longer exposure times were used to compensate. The resulting OVIRS spatial resolution was  $\sim 4$  to 5 m cross-track and  $\sim 7$  to 10 m along-track, plus the surface projection effects at the higher latitudes. We produced spectral maps of these smaller regions at  $\sim 60\text{-m}^2$  areal resolution.

### Globally averaged spectra

Global spectra were calculated for each Detailed Survey equatorial spectral mapping station by averaging all OVIRS spots that were fully on the surface; there are 6189, 7193, and 6877 spectra for 10:00 a.m., 12:30 p.m., and 3:00 p.m., respectively. Although not identical to a full-disk spectrum, because of the fixed local time, the averages include emission angles from latitudes all the way to the poles. In the 12:30 p.m. data, Benu shows a weak global absorption feature from 3.2 to 3.6  $\mu\text{m}$  (hereafter, the 3.4- $\mu\text{m}$  feature), which we attribute to carbonate and organic materials (Fig. 1B). This absorption feature was not detectable in full-disk, unresolved OVIRS spectra, taken when Benu only filled  $\sim 40\%$  of the field of view and the surface was warmer owing to closer proximity to the Sun (9). Spatially resolved datasets were also acquired in March 2019, very close to Benu's perihelion. These contain hits of a 3.4- $\mu\text{m}$  absorption feature, but the band depth was likely affected by thermal fill-in, an effect whereby greater thermal emission at high temperatures increases the thermal flux at the band wavelength, thereby weakening absorption features (17). Those spectra were also noisier

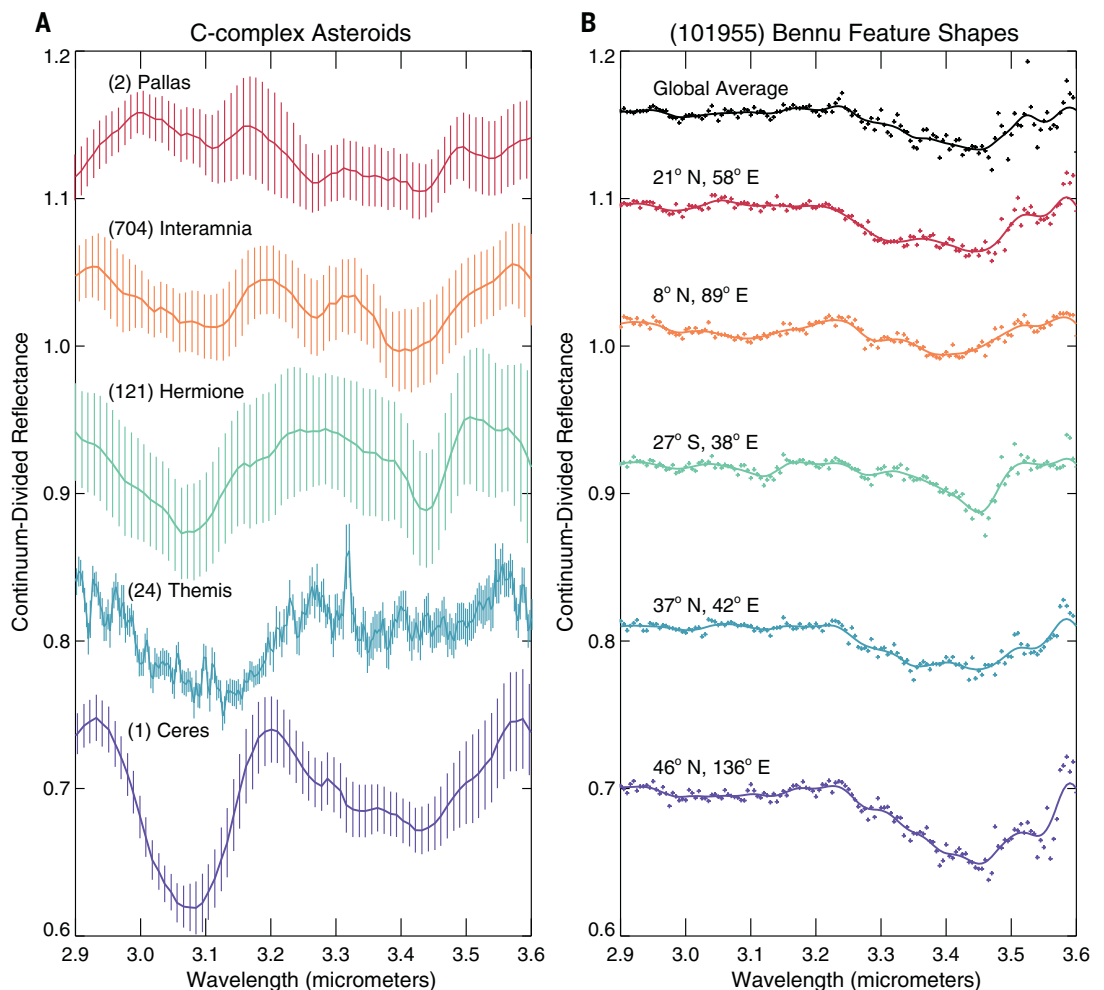
at long wavelengths  $> 3 \mu\text{m}$ , owing to higher instrument detector temperatures.

Benu's globally averaged 3.4- $\mu\text{m}$  absorption feature, as observed during the Detailed Survey, is distinct from that seen on other C-complex asteroids (Fig. 1). Previous observations of a 3.4- $\mu\text{m}$  feature in other disk-integrated asteroid spectra, including (24) Themis and Themis-like asteroids, have been attributed primarily to aliphatic organic molecules (18–20). However, ground-based observations of (1) Ceres and Ceres-like asteroids have revealed a strong 3.4- $\mu\text{m}$  feature that was instead primarily attributed to carbonates, as it was accompanied by a detection of the 3.9- $\mu\text{m}$  carbonate band (20, 21). Several main-belt asteroids display variability between 3.2 and 3.6  $\mu\text{m}$ , indicating potential compositional variation, although the band variations are uncertain for (704) Interamnia and (121) Hermione (Fig. 1A) (18, 22). However, in individual spot spectra, Benu has absorption band shapes between 3.2 and 3.6  $\mu\text{m}$  that are similar to those of Themis, Ceres, and other main-belt asteroids (Fig. 1B).

We also produced a globally averaged thermal infrared spectrum using data from the

### Fig. 1. Comparison of 3.4- $\mu\text{m}$ absorption features on main-belt asteroids and multiple locations on Benu.

(A) C-complex asteroid spectra obtained at  $15^\circ$  to  $30^\circ$  phase angle (22)—except the (24) Themis data from (18)—each plotted with  $1\sigma$  uncertainties. Curves are offset from 1.0 for clarity. (B) The OVIRS globally averaged Benu spectrum at  $9^\circ$  phase angle shows a broad absorption feature of  $\sim 2\%$  depth, extending from 3.2 to 3.6  $\mu\text{m}$ . The solid line shows the spectrum smoothed with a nine spectral channel-width Gaussian. Spectra of individual locations on Benu are also shown, the coordinates of each location labeled, and curves are offset from 1.0 for clarity. Uncertainties are smaller than the symbol size.



OSIRIS-REx Thermal Emission Spectrometer (OTES) (23), acquired during the Detailed Survey phase, to search for spectral features that could be attributable to carbon in organics and/or carbonates. However, other minerals exhibit features in the same spectral region, complicating our interpretation. The radiometric performance of OTES is degraded at  $>1300\text{ cm}^{-1}$  ( $\lesssim 7.7\text{ }\mu\text{m}$ ) and at surface temperatures lower than 325 K (23), requiring us to co-add spectra to maintain an adequate signal-to-noise ratio (fig. S1) (24). This prevents us from obtaining detailed spatial distribution information for comparison with the OVIRS observations made at four times the areal resolution. We therefore limit our analyses to just the OVIRS data.

### Feature repeatability

With repeated coverage over some areas of Bennu's surface, we investigated the effects of phase angle on spectral shape to determine whether the absorption is an observational or processing artifact. The globally averaged spectra from the three local solar times are shown in Fig. 2A. A similar 3.4- $\mu\text{m}$  band shape is seen in each average spectrum, although at 12:30 p.m. and 3:00 p.m. the feature is slightly deeper near 3.45  $\mu\text{m}$  and has more absorption below 3.3  $\mu\text{m}$  than at 10:00 a.m. There is no apparent thermal emission fill-in in the absorption band at any phase angle, because the average surface temperatures were low (328 K at 12:30 p.m.); however, individual hot surface locations become very noisy in the 3:00 p.m. spectra. Using the average surface temperatures, reflectance, and solar range-corrected flux for each observation, the radiance contribution from reflected solar light at 3.4  $\mu\text{m}$  is shown to be ~31, 22, and 15% for 10:00 a.m., 12:30 p.m., and 3:00 p.m., respectively. However, the absolute reflected solar radiance at 12:30 p.m. is nearly twice that at 10:00 a.m. and 3:00 p.m., resulting in the highest signal-to-noise ratio after thermal tail subtraction (fig. S2) (24).

We also investigated feature repeatability on a regional scale. Using the regions with higher-resolution observations (Fig. 2B), we averaged several overlapping spots together to obtain a close (although not identical) match to the spatial resolution of each Detailed Survey map. Two overlapping spots in each observation cover ~900  $\text{m}^2$ , and the afternoon spectra again have a deeper band than the 10:00 a.m. spectra, but spectral shapes are similar for each observation. We also compared the average of all high-spatial-resolution spots over an area with the corresponding low-spatial-resolution spectrum (Fig. 2, C and D). Although the spectra were taken at different local solar times, differences between the resulting spectra are  $<0.5\%$ , indicating that phase angle does not appreciably affect the band depth or shape.

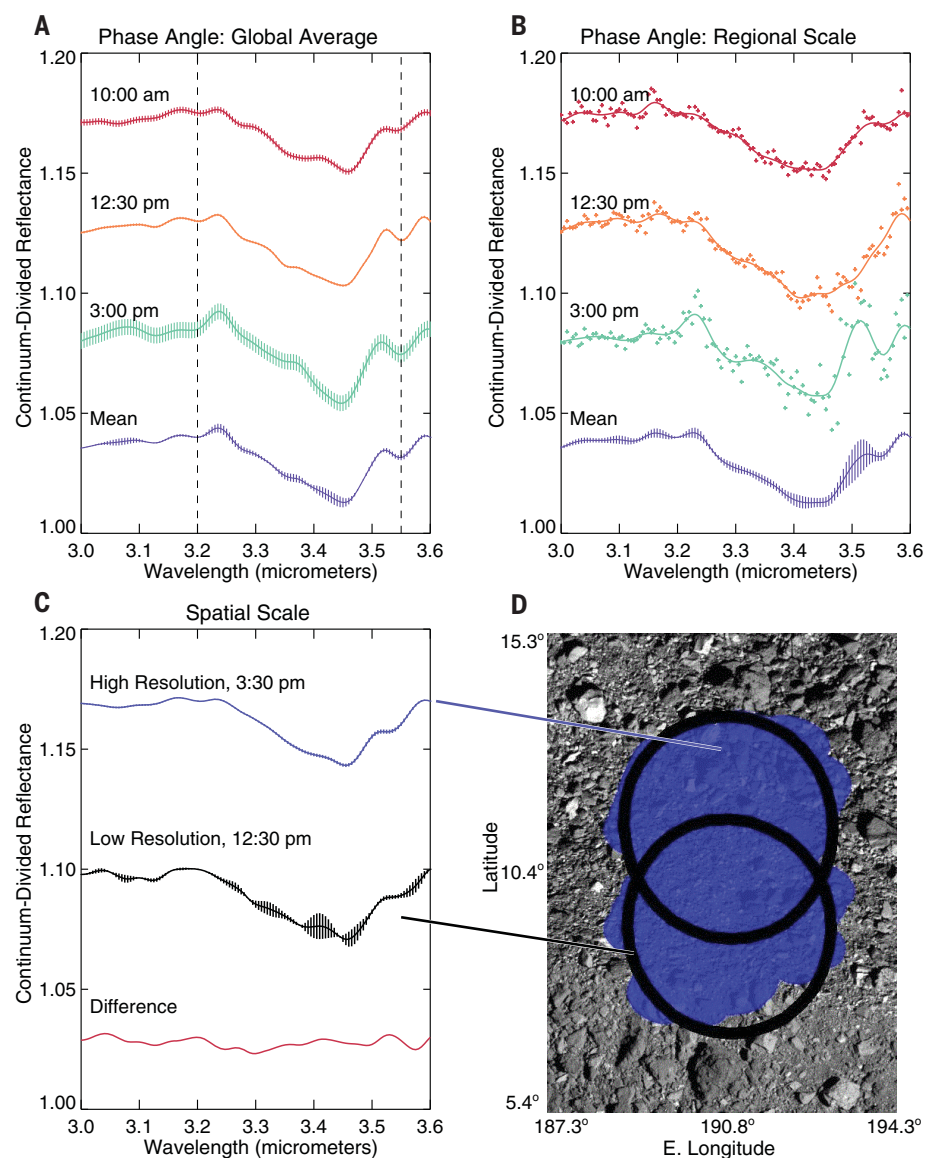


**Fig. 2. Effect of local solar time (phase angle) and spatial scale on absorption feature shapes and depths.** (A) Globally averaged spectra at 10:00 a.m. ( $\sim 30^\circ$  phase), 12:30 p.m. ( $\sim 9^\circ$ ), and 3:00 p.m. ( $45^\circ$ ) local solar time, and the mean across all three phase angles; hatching indicates the standard error of the mean. (B) Regional-scale ( $\sim 900\text{ m}^2$ ) spectra at the same phase angles as the global spectra, and their mean with standard error (hatching). Points show the data, and lines are after smoothing with a nine spectral channel-width Gaussian. (C) Average of 163 local spectra (blue) compared with a regional two-spectrum average (black) and their difference (red); spectra are plotted as Gaussian-smoothed curves (lines) with standard error (hatching). (D) Approximate areas covered by the observations shown in (C), but without vertical along-track smear, which improves the overlap between the regional (black empty circles) and local (blue filled circles) spectral spots.

### Global surface distribution

To map the distribution of the absorption feature across the surface, we used the 12:30 p.m. spectra, as they have the highest signal-to-noise ratio and fewest shadows. From those data, we calculated the band area (band depth integrated from 3.2 to 3.6  $\mu\text{m}$ ), mapped it onto the surface of a three-dimensional shape model of Bennu (25), and overlaid the results on an OSIRIS-REx Camera Suite (OCAMS) base map with 5-cm spatial resolution (26, 27) (Fig. 3A).

Band area was chosen over single-channel band depth to cover the range of spectral shapes that could arise as a result of different carbonates or organics (28).

The map in Fig. 3A shows that carbon-bearing material is spread over 98% of Bennu's surface, with band areas varying from 0.12 to 0.82%  $\mu\text{m}$ , but in no discernible large-scale pattern; 98% of the surface between  $\pm 50^\circ$  latitude shows a band depth of  $>1\%$  at 3.42  $\mu\text{m}$ , and 32% of the surface has an absorption  $\geq 2\%$ . Most other

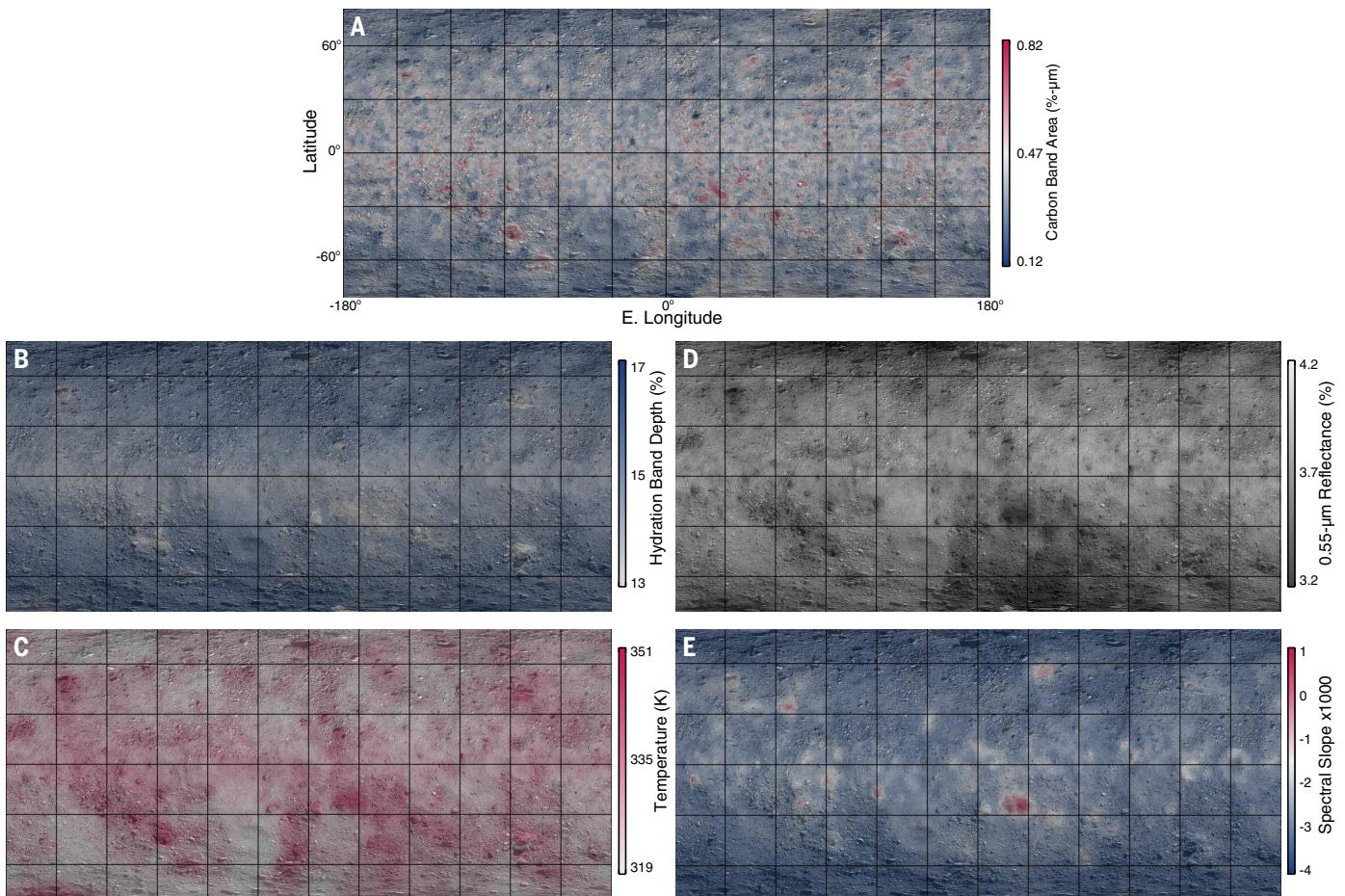


**Fig. 3. Global spectral maps of Bennu from the OVIRS observations taken at the 12:30 p.m. Equatorial Station.** (A) Band area from 3.2 to 3.6  $\mu\text{m}$ , showing absorption due to carbon-bearing materials. (B) 2.74- $\mu\text{m}$  hydration band depth, (C) effective surface temperature, (D) 0.55- $\mu\text{m}$  reflectance, and (E) spectral slope from 0.5 to 1.5  $\mu\text{m}$ . The latitude and longitude grid shown in (A) is overlaid on the other panels.

surface parameters, such as 12:30 p.m. surface temperature, 0.55- $\mu\text{m}$  reflectance, or visible spectral slope (Fig. 3, B to D), align with surface features: the darkest boulders and blanketed areas (lowest 0.55- $\mu\text{m}$  reflectance) tend to be the hottest and have the shallowest hydration band at 2.74  $\mu\text{m}$ . The boulders appear to have low thermal inertia, high thermal roughness, and usually a redder spectral slope (29, 30).

Over wavelengths from 0.5 to 1.5  $\mu\text{m}$ , most of the surface has a blue (negative) spectral slope (8, 9), but some individual regions have a redder (flat to slightly positive) slope (Fig. 3E). Some individual boulders stand out in the spectral slope map, but not all boulders are redder than average; some are bluer (steeper negative slope). These data agree with photometric color observations at higher spatial resolution, which show that individual boulders and craters have a variety of colors (30). Many of the areas that are redder than average occur at low latitudes, in agreement with some ground-based measurements that find equatorial reddening, although the measured

variation in slope in OVIRS data is much smaller than is seen in those studies (31). As with the 3.4- $\mu\text{m}$  absorption, the range of spectral behavior observed on Bennu at wavelengths shorter than 2.5  $\mu\text{m}$  is similar to that found among B-type asteroids throughout the main belt (5). Bennu's blue color may in part be due to space weathering (30).

To determine whether Bennu's global characteristics are correlated at low spatial resolution, we calculated Spearman's rank correlation values,  $r$ , on different map pairs. We limited the calculation to latitudes less than  $50^\circ$  to avoid effects from variable solar illumination on short wavelength and thermal parameters, which affect high latitudes more strongly; at this limit, the temperature map has weak correlation to incidence or emission angles ( $|r| < 0.25$ ), and further narrowing the latitude range did not meaningfully affect the results. At low phase angle, maps of the 2.74- $\mu\text{m}$  hydration band depth and 0.55- $\mu\text{m}$  reflectance show some correlation with peak surface temperature ( $|r| = 0.76$  and  $0.65$ , respectively) (fig. S3) (24). The slope from 0.5 to 1.5  $\mu\text{m}$  shows the

least correlation with peak temperature, with the bluest and the reddest regions both being warmer than the average. However, the spectral slope does weakly correlate with the hydration band and 0.55- $\mu\text{m}$  reflectance ( $|r| > 0.55$ ), with the reddest large boulders having the shallowest hydration band and the lowest reflectance.

Although the 3.2- to 3.6- $\mu\text{m}$  band area map shows that some boulders have a deeper absorption than others, comparison with other surface parameters (24) indicates no obvious correlation, and all map pairs have  $|r| \leq 0.45$ . Bennu's carbon band area follows neither the reddest nor the darkest regions on the surface. This would be unexpected if Bennu's 3.4- $\mu\text{m}$  band were attributable entirely to organics (32). However, as most spectra have an absorption shape that matches a mix of organics and carbonates (28), we cannot globally map these independently of one another. Thus, the lack of correlation may be the result of composition or for another reason, such as particle size effects.

As the 0.55- $\mu\text{m}$  albedo and hydration band depth are correlated with surface temperature, we also produced a detrended 2.74- $\mu\text{m}$

hydration band map (fig. S4) to search for residual variations after removing the temperature dependence (24). Neither the band area from 3.2 to 3.6  $\mu\text{m}$  nor the spectral slope from 0.5 to 1.5  $\mu\text{m}$  show any correlation with the detrended hydration map, with  $|r| \leq 0.23$  (24). The 2.74- $\mu\text{m}$  hydration band map, caused by the presence of hydrated phyllosilicates, shows a correlation with latitude,  $|r| = 0.58$  (fig. S5). This correlation decreases to  $|r| = 0.48$  in the temperature-detrended map. The correlations between hydration band and peak surface temperature or latitude could be due to dehydration, differential space weathering, compositional differences, particle size, surface roughness, or other causes. Although hydrated phyllosilicates and carbon-bearing material are globally present, their lack of correlation indicates separate formation processes.

### Local variability

At the 20- to 30-m spot scale used in the global maps, spot-to-spot variability in band area ( $0.04 \pm 0.01$  to  $0.84 \pm 0.02\%$   $\mu\text{m}$ ) indicates a heterogeneous surface, either in terms of band depth or shape. At the 5- to 10-m scale, the band shape and area are consistent over small areas where the spots overlap on a geologic feature (Fig. 4B) but change as the spots move to adjacent rocks, possibly because of local variability (Fig. 4, A and C). However, some of these high-spatial-resolution data were acquired at phase angles where shadows may affect the signal, particularly at high latitudes or near large boulders (Fig. 4A).

Nonetheless, at the finer spatial scale, absorption depths exceed 10% in a few isolated locations; these locations with the deepest absorptions likely have the highest concentra-

tion of carbon-bearing material, although viewing conditions and particle size effects may also affect band depth. While full global coverage was not obtained at this resolution, 187 spectra (~1% of the high-spatial-resolution spots) were found to have absorptions of 5 to 14% at 3.42, 3.45, or 3.47  $\mu\text{m}$ ; these wavelengths were chosen to span the deepest absorption wavelengths for a mix of organics and carbonates (28). Most of these locations occur over boulders; only a single spectrum with a deep absorption feature occurs over a smooth crater floor, which is ringed by boulders having deep absorptions. However, this region is at high latitude, and the viewing conditions included some large shadows.

To avoid potential effects on band depth caused by shadows and low signal, we identified 18 low-latitude spectra with a 3.4- $\mu\text{m}$  absorption

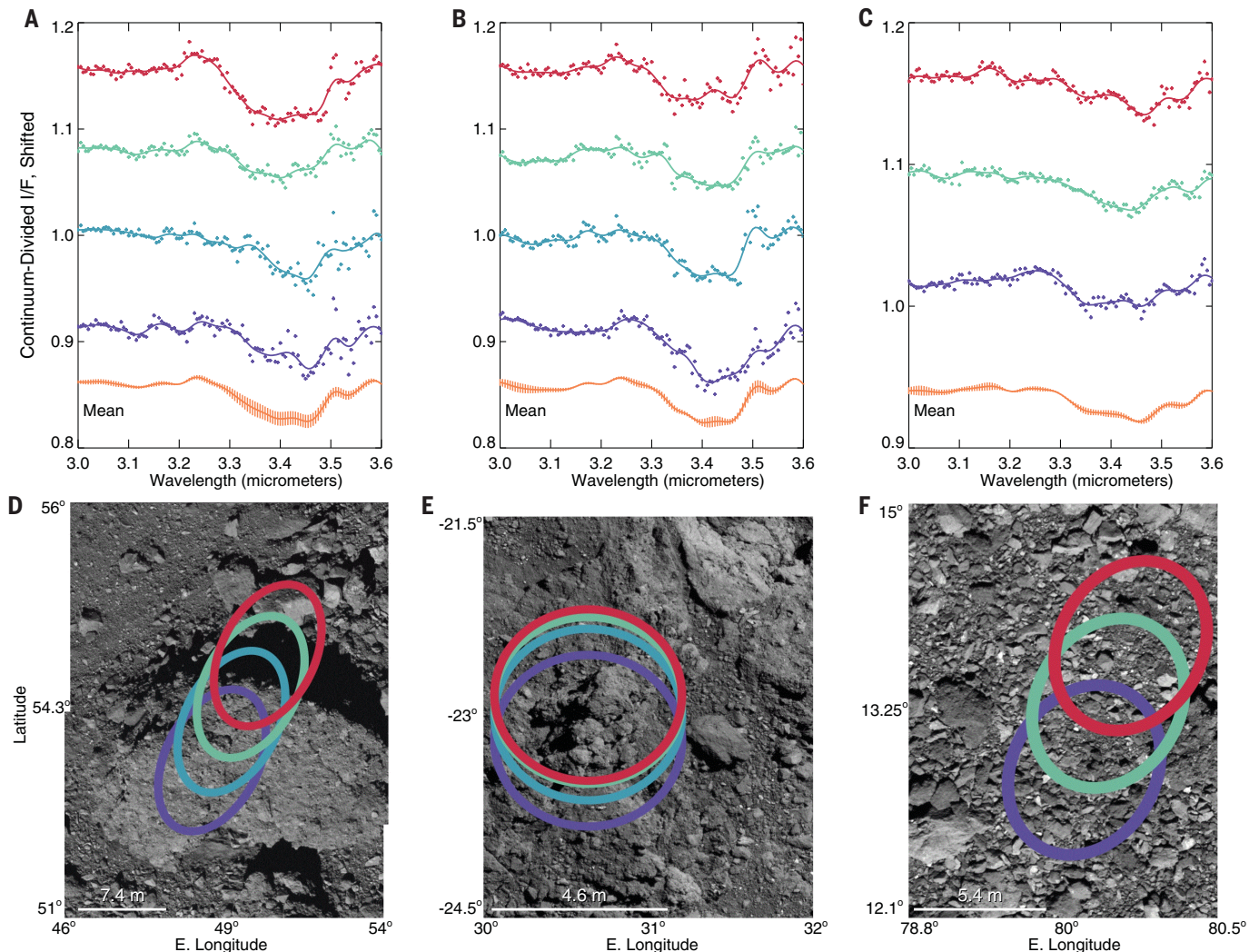


**Fig. 4. Individual high-areal-resolution (~60 m<sup>2</sup>) local spectra and their corresponding OVIRS footprints.** (A to C) Spectra of selected locations and their means. (D to F) The corresponding OVIRS footprints (ellipses, elongated by along-track motion) overlaid on OCAMS panchromatic images acquired at the same time. In (A), a deep absorption feature changes spectral shape and depth as the field of view moves off a large boulder and onto smaller boulders (D), which could have different composition, and the mean shows variation over the full band. In (B), a cluster of spectra over a rock pile (E) shows consistent shapes with less variation in the mean than in (A). In (C), a region with little absorption shows few large boulders in the field of view (F) and similar variation in the mean as (B).

feature >5% in depth and overlaid them on the OCAMS map of Bennu (26, 27). In some instances, the spots overlap spatially, resulting in 10 individual locations with deep 3.4- $\mu\text{m}$  absorption (Fig. 5A). All of these locations lie on large boulders that dominate the OVIRS field of view. As with the global-scale maps, these boulders span a range of brightness and colors, with no distinguishing morphological features; some appear buried or are composites of broken material, whereas others are neither (30). Another low-latitude region (Fig. 5B) shows that the deepest absorptions occur in a rock field between two craters. In comparison, the OSIRIS-REx mission's primary sample site, Nightingale crater at 56°N, 42°E (Fig. 5C), shows many spots with 3.4- $\mu\text{m}$  absorption of 5 to 7% depth, despite low solar illumination. Again, although there is an ab-

sorption over the entire region, most spots with deep features correspond to boulders around the rim of the crater (28).

#### Origin of carbon material

The variation in 3.4- $\mu\text{m}$  feature shape depends on surface location, with individual spot spectra that match those of other C-complex asteroids (Fig. 1A), demonstrating a heterogeneity that spans multiple asteroid families and classes. This heterogeneity is likely caused by varying proportions of carbonate and organics (28), which we cannot distinguish in our global dataset. A spectral feature we observe at 3.98  $\mu\text{m}$  may be due to carbonates (28) (Fig. 6), but the signal-to-noise ratio of the thermal-corrected spectra is <25 above 3.7  $\mu\text{m}$  (24). An observed 2.3- $\mu\text{m}$  feature could also be due to carbonates or to phyllosilicates, but the lack of a corre-

sponding 2.5- $\mu\text{m}$  absorption makes an identification uncertain. Spectral slopes could be affected by the presence of organics (33), but Bennu's spectral slope variation is small, and redder OVIRS spectra show similar absorption features to bluer spectra in the low-resolution 600  $\text{m}^2$  data (Fig. 6).

We do not observe widespread evidence of a 3.1- $\mu\text{m}$  absorption from water ice or ammoniated phyllosilicates (Fig. 1B), which is present on many C-complex main-belt asteroids (e.g., Ceres and Themis) (18, 22), indicating that Bennu's bulk mineralogy and chemistry are distinct, despite the similarities in the 3.4- $\mu\text{m}$  region. As a rubble-pile near-Earth asteroid, Bennu is a mixture of parent-body material aggregates that have been warmed by proximity to the Sun, which would have removed volatile water ice (34).

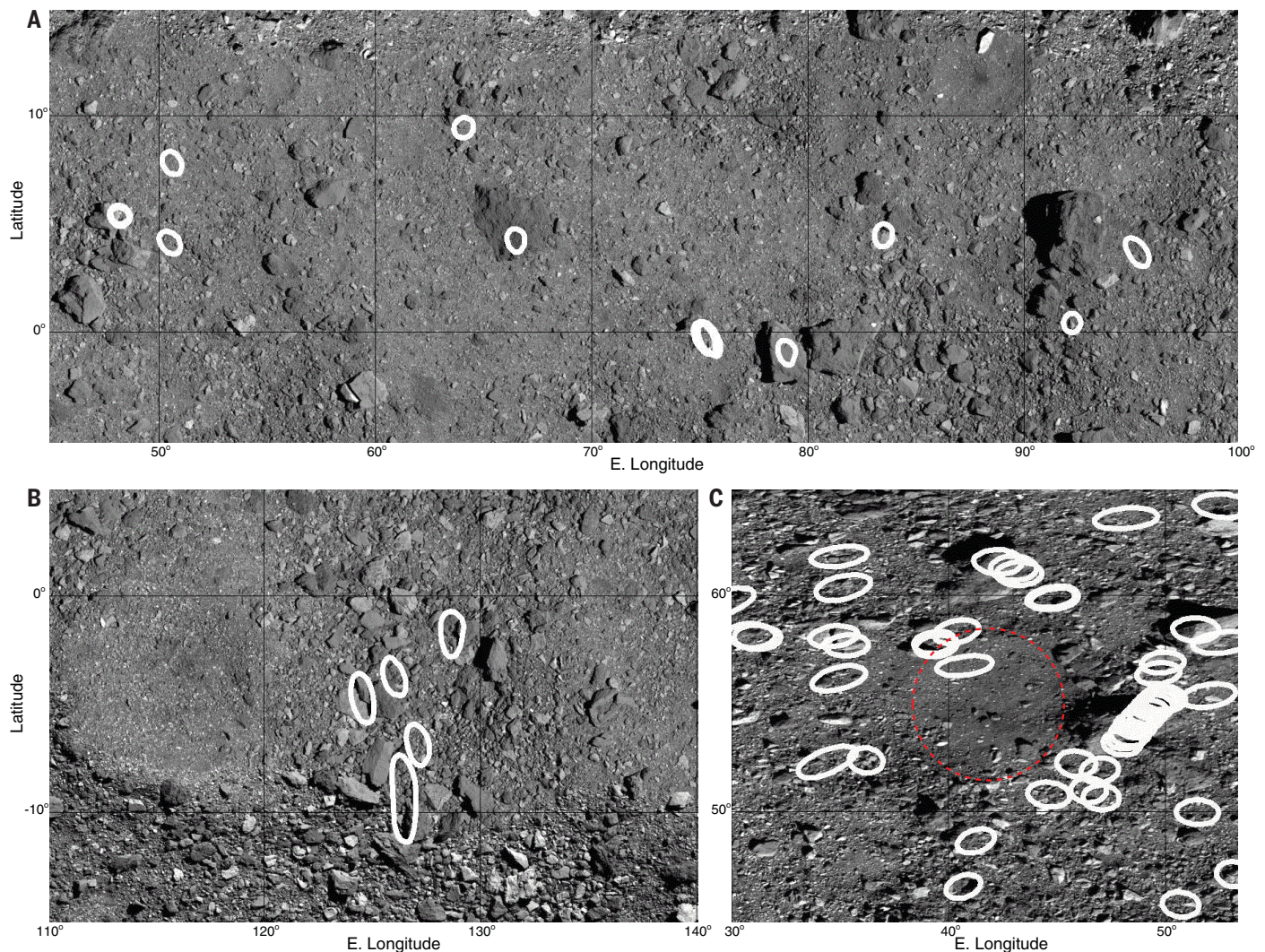
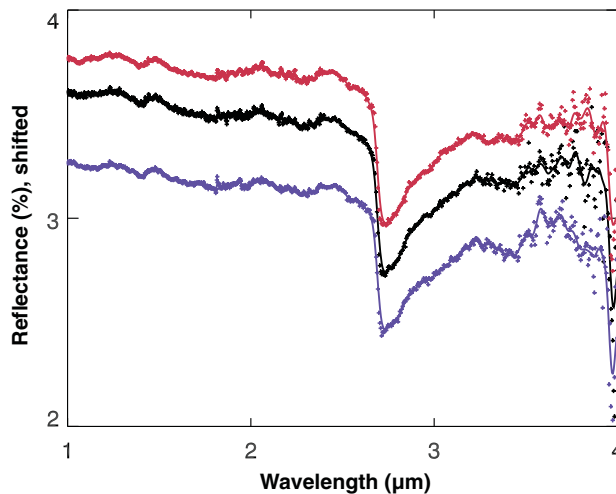


**Fig. 5. The locations and sizes of OVIRS footprints (white outlines) of spectra with single-channel absorptions >5% at either 3.42, 3.45, or 3.47  $\mu\text{m}$ .** The footprints are overlaid on the 5-cm-resolution base map (26, 27); they are elongated by surface projection effects but neglect along-track smear. Footprint coverage over the images is sparse, primarily in separated north-south scans. (A) Low latitudes show a number of deep absorptions, primarily over boulders. (B) An adjacent equatorial region shows that the boulders between two craters also have deep absorptions. (C) The environs around the OSIRIS-REx primary sample site, Nightingale crater (red dashed circle), also show locally deeper absorptions.

**Fig. 6. Bennu reflectance spectra from 2 to 4  $\mu\text{m}$ .**

The global average spectrum (black curve) shows other absorption features centered near 2.3 and 3.98  $\mu\text{m}$ . There is little difference in the reflectance spectrum of any spot, regardless of spectral slope from 0.5 to 1.5  $\mu\text{m}$ , with redder regions (red curve) showing the same spectral features as bluer regions (blue curve). The red and blue curves are shifted by 0.2 for clarity.



Local regions on Ceres have complex mineralogy including organic matter, carbonates, and ammoniated phases (33, 35). Ground-based observations of Ceres indicated the presence of carbonates, while orbital data showed several organic-rich areas (32, 36). The limited spatial concentration of aliphatic organics on Ceres has been attributed to geologically recent exposure of those materials, such that they have not been broken down by solar irradiation (33, 35, 37). With irradiation, aliphatic carbon breaks down to graphitized or amorphous carbon, and these phases are thought to be ubiquitous on Ceres (38); they may also be present on Bennu (29) but cannot be directly observed with NIR spectroscopy. The widespread presence of aliphatic organics at 3.4  $\mu\text{m}$  would indicate that neither space weathering nor heating on Bennu were pervasive enough to degrade (or graphitize) all aliphatic organics. To preserve a widespread 3.4- $\mu\text{m}$  organic feature, most of the material on Bennu's surface could not have been exposed to the space environment for more than a few million years (39–41).

Two scenarios could explain the carbon-bearing material on Bennu's surface and its variety of spectral shapes: accretion of external material over time or gradual exposure of a mix of materials present from its aggregation. First, given the similarity of local-area spectral shapes to different C-complex asteroids, Bennu's surface may exhibit a mix of materials accreted during its time in the main belt and later transit to a near-Earth orbit (exogenous material). Pyroxene-bearing boulders have been detected on the surface and are spectrally consistent with the howardite, eucrite, and diogenite achondrite meteorite groups associated with asteroid (4) Vesta (42), indicating that the surface retains at least some exogenous material. However, at the scale of these observations (~20 m per spot), there is no obvious connection between the carbon-bearing absorption features and any particu-

lar rock type (30). The meteorites that are the closest spectral analogs to Bennu (CI and CM chondrites) tend to have less than 5 vol % carbonates. Carbon-bearing materials were likely ubiquitous in the forming solar system and interstellar medium, so they would have been available to form organics and carbonates in planetesimals (43). Any such material delivered to the surface of Bennu would be altered by space weathering and high surface temperatures, especially during perihelion, so pristine carbon-bearing material, particularly organics, would not be preserved unless synthesized and delivered within the past million years (39–41). The widespread distribution of such material on Bennu's surface makes this scenario unlikely.

Alternatively, as a rubble pile formed after a collision (2, 25), Bennu's surface may be peppered with boulders aggregated from different layers of its parent body and/or the impactor. Again, any surface materials, especially organics, would degrade over time. It is possible that buried organic material is being newly exposed by surface impacts, although we do not observe any correlation between the carbon-bearing material and craters (Figs. 3 and 5).

In the carbon-bearing boulders, thermal cycling and degradation by meteoroid impacts could cause fatigue and fracturing that exposes new organic material over time (44, 45). The ejection of particles from Bennu's surface supports the idea that fresh surfaces are actively being exposed (46). Bennu's blue spectral slope is also consistent with the colors of a subset of asteroids that show evidence of ongoing mass loss and are known as main-belt comets. However, on Bennu, this blue spectral slope extends to the shortest wavelengths we observe, which is rare for main-belt comets (19). Conversely, some of Bennu's boulders display veins that may be composed of carbonate minerals (28), lending further credence to the supposition that we are observing a mixture of carbon-bearing materials.

Our observations provide context for the sample planned to be returned to Earth by OSIRIS-REx. The widespread surface distribution of the 3.4- $\mu\text{m}$  absorption on Bennu indicates that the sample should contain carbon-bearing material, regardless of sampling location. The primary sample site, Nightingale, shows deeper regional carbon-bearing absorptions than average, particularly in the boulders around the crater rim; this does not rule out substantial carbon-bearing material on the crater floor.

### Methods summary

All OVIRS spectra were calibrated using an automated pipeline that converts raw counts to calibrated radiance units (watts per square centimeter per micrometer per steradian) (24, 47). Before analysis, each spectrum was resampled onto a common wavelength axis with 2-nm spectral resolution below 2.4  $\mu\text{m}$  and 5-nm resolution from 2.4 to 4.3  $\mu\text{m}$ . These resampled spectra were then fitted with a model of a thermal tail, which was subtracted, then divided by the solar flux to produce reflectance spectra (24). Surface feature maps were constructed using a Lommel-Seeliger disk correction to remove latitudinal effects. For band depth and shape comparisons, the background continuum was removed using a model fitted to each spectrum (24).

### REFERENCES AND NOTES

1. D. N. DellaGiustina *et al.*, Properties of rubble-pile asteroid (101955) Bennu from OSIRIS-REx imaging and thermal analysis. *Nat. Astron.* **3**, 341–351 (2019). doi: [10.1038/s41550-019-0731-1](https://doi.org/10.1038/s41550-019-0731-1)
2. D. S. Lauretta *et al.*, The OSIRIS-REx target asteroid (101955) Bennu: Constraints on its physical, geological, and dynamical nature from astronomical observations. *Meteorit. Planet. Sci.* **50**, 834–849 (2015). doi: [10.1111/maps.12353](https://doi.org/10.1111/maps.12353)
3. D. J. Tholen, "Asteroid taxonomy from cluster analysis of photometry," thesis, University of Arizona, Tucson (1984).
4. S. J. Bus, P. R. Binzel, Phase II of the Small Main-Belt Asteroid Spectroscopic Survey, A feature-based taxonomy. *Icarus* **158**, 146–177 (2002). doi: [10.1006/icar.2002.6856](https://doi.org/10.1006/icar.2002.6856)
5. J. de León, N. Pinilla-Alonso, H. Campins, J. Licandro, G. A. Marzo, Near-infrared spectroscopic survey of B-type asteroids: Compositional analysis. *Icarus* **218**, 196–206 (2012). doi: [10.1016/j.icarus.2011.11.024](https://doi.org/10.1016/j.icarus.2011.11.024)
6. D. S. Lauretta *et al.*, OSIRIS-REx: Sample return from asteroid (101955) Bennu. *Space Sci. Rev.* **212**, 925–984 (2017). doi: [10.1007/s11214-017-0405-1](https://doi.org/10.1007/s11214-017-0405-1)
7. B. E. Clark *et al.*, Spectroscopy of B-type asteroids: Subgroups and meteorite analogs. *J. Geophys. Res.* **115**, E06005 (2010). doi: [10.1029/2009JE003478](https://doi.org/10.1029/2009JE003478)
8. B. E. Clark *et al.*, Asteroid (101955) 1999 RQ36: Spectroscopy from 0.4 to 2.4  $\mu\text{m}$  and meteorite analogs. *Icarus* **216**, 462–475 (2011). doi: [10.1016/j.icarus.2011.08.021](https://doi.org/10.1016/j.icarus.2011.08.021)
9. V. E. Hamilton *et al.*, Evidence for widespread hydrated minerals on asteroid (101955) Bennu. *Nat. Astron.* **3**, 332–340 (2019). doi: [10.1038/s41550-019-0722-2](https://doi.org/10.1038/s41550-019-0722-2); pmid: [31360777](https://pubmed.ncbi.nlm.nih.gov/31360777/)
10. W. F. Bottke *et al.*, In search of the source of asteroid (101955) Bennu: Applications of the stochastic YORP model. *Icarus* **247**, 191–217 (2015). doi: [10.1016/j.icarus.2014.09.046](https://doi.org/10.1016/j.icarus.2014.09.046)
11. H. Campins *et al.*, The origin of asteroid 101955 (1999 RQ36). *Astrophys. J.* **721**, L53–L57 (2010). doi: [10.1088/2041-8205/721/1/L53](https://doi.org/10.1088/2041-8205/721/1/L53)
12. N. Pinilla-Alonso *et al.*, Portrait of the Polana-Eulalia family complex: Surface homogeneity revealed from near-infrared spectroscopy. *Icarus* **274**, 231–248 (2016). doi: [10.1016/j.icarus.2016.03.022](https://doi.org/10.1016/j.icarus.2016.03.022)
13. S. Sugita *et al.*, The geomorphology, color, and thermal properties of Ryugu: Implications for parent-body processes.

- Science **364**, eaaw0422 (2019). doi: [10.1126/science.aaw0422](https://doi.org/10.1126/science.aaw0422); pmid: [30890587](https://pubmed.ncbi.nlm.nih.gov/30890587/)
14. K. Kitazato *et al.*, The surface composition of asteroid 162173 Ryugu from Hayabusa2 near-infrared spectroscopy. *Science* **364**, 272–275 (2019). doi: [10.1126/science.aaw7432](https://doi.org/10.1126/science.aaw7432); pmid: [30890589](https://pubmed.ncbi.nlm.nih.gov/30890589/)
  15. H. Campins *et al.*, Spectra of asteroid families in support of Gaia. *Planet. Space Sci.* **73**, 95–97 (2012). doi: [10.1016/j.pss.2012.06.017](https://doi.org/10.1016/j.pss.2012.06.017)
  16. D. C. Reuter *et al.*, The OSIRIS-REx Visible and InfraRed Spectrometer (OVIRS): spectral maps of the asteroid Bennu. *Space Sci. Rev.* **214**, 54 (2018). doi: [10.1007/s11214-018-0482-9](https://doi.org/10.1007/s11214-018-0482-9)
  17. B. Hapke, “Thermal emission and emission spectroscopy” in *Theory of Reflectance and Emittance Spectroscopy* (Cambridge Univ. Press, ed. 2, 2012), pp. 412–439.
  18. A. S. Rivkin, J. P. Emery, Detection of ice and organics on an asteroidal surface. *Nature* **464**, 1322–1323 (2010). doi: [10.1038/nature09028](https://doi.org/10.1038/nature09028); pmid: [20428165](https://pubmed.ncbi.nlm.nih.gov/20428165/)
  19. H. Campins *et al.*, Water ice and organics on the surface of the asteroid 24 Themis. *Nature* **464**, 1320–1321 (2010). doi: [10.1038/nature09029](https://doi.org/10.1038/nature09029); pmid: [20428164](https://pubmed.ncbi.nlm.nih.gov/20428164/)
  20. A. S. Rivkin, E. S. Howell, J. P. Emery, Infrared spectroscopy of large, low-albedo asteroids: Are Ceres and Themis archetypes or outliers? *J. Geophys. Res. Planets* **124**, 1393–1409 (2019). doi: [10.1029/2018JE005833](https://doi.org/10.1029/2018JE005833)
  21. A. S. Rivkin, E. L. Volquardsen, B. E. Clark, The surface composition of Ceres: Discovery of carbonates and iron-rich clays. *Icarus* **185**, 563–567 (2006). doi: [10.1016/j.icarus.2006.08.022](https://doi.org/10.1016/j.icarus.2006.08.022)
  22. F. Usui, S. Hasegawa, T. Ootsubo, T. Onaka, AKARI/IRC near-infrared asteroid spectroscopic survey: AcuA-spec. *Publ. Astron. Soc. Jpn.* **71**, 1–41 (2019). doi: [10.1093/pasj/psy125](https://doi.org/10.1093/pasj/psy125)
  23. P. R. Christensen *et al.*, The OSIRIS-REx Thermal Emission Spectrometer (OTES) instrument. *Space Sci. Rev.* **214**, 87 (2018). doi: [10.1007/s11214-018-0513-6](https://doi.org/10.1007/s11214-018-0513-6)
  24. Materials, methods, and related figures are available as supplementary materials.
  25. O. S. Barnouin *et al.*, Shape of (101955) Bennu indicative of a rubble pile with internal stiffness. *Nat. Geosci.* **12**, 247–252 (2019). doi: [10.1038/s41561-019-0330-x](https://doi.org/10.1038/s41561-019-0330-x); pmid: [31080497](https://pubmed.ncbi.nlm.nih.gov/31080497/)
  26. B. Rizk *et al.*, OCAMS: The OSIRIS-REx Camera Suite. *Space Sci. Rev.* **214**, 26 (2018). doi: [10.1007/s11214-017-0460-7](https://doi.org/10.1007/s11214-017-0460-7)
  27. C. A. Bennett *et al.*, A high-resolution global basemap of (101955) Bennu. *Icarus* **113690** (2020). doi: [10.1016/j.icarus.2020.113690](https://doi.org/10.1016/j.icarus.2020.113690)
  28. H. H. Kaplan *et al.*, Bright carbonate veins on asteroid (101955) Bennu: Implications for aqueous alteration history. *Science* **370**, eabc3557 (2020). doi: [10.1126/science.abc3557](https://doi.org/10.1126/science.abc3557); pmid: [33033155](https://pubmed.ncbi.nlm.nih.gov/33033155/)
  29. B. Rozitis *et al.*, Asteroid (101955) Bennu’s weak boulders and thermally anomalous equator. *Sci. Adv.* **6**, eabc3699 (2020). doi: [10.1126/sciadv.abc3699](https://doi.org/10.1126/sciadv.abc3699); pmid: [33033037](https://pubmed.ncbi.nlm.nih.gov/33033037/)
  30. D. N. DellaGiustina *et al.*, Variations in color and reflectance on the surface of asteroid (101955) Bennu. *Science* **370**, eabc3660 (2020). doi: [10.1126/science.abc3660](https://doi.org/10.1126/science.abc3660); pmid: [33033157](https://pubmed.ncbi.nlm.nih.gov/33033157/)
  31. R. P. Binzel *et al.*, Spectral slope variations for OSIRIS-REx target Asteroid (101955) Bennu: Possible evidence for a fine-grained regolith equatorial ridge. *Icarus* **256**, 22–29 (2015). doi: [10.1016/j.icarus.2015.04.011](https://doi.org/10.1016/j.icarus.2015.04.011)
  32. C. M. Pieters *et al.*, Geologic constraints on the origin of red organic-rich material on Ceres. *Meteorit. Planet. Sci.* **53**, 1983–1998 (2018). doi: [10.1111/maps.13008](https://doi.org/10.1111/maps.13008)
  33. H. H. Kaplan, R. E. Milliken, C. M. O’D. Alexander, New constraints on the abundance and composition of organic matter on Ceres. *Geophys. Res. Lett.* **45**, 5274–5282 (2018). doi: [10.1029/2018GL077913](https://doi.org/10.1029/2018GL077913)
  34. B. Rozitis *et al.*, Implications for ice stability and particle ejection from high-resolution temperature modeling of asteroid (101955) Bennu. *J. Geophys. Res. Planets* **125**, (2020). doi: [10.1029/2019JE006323](https://doi.org/10.1029/2019JE006323)
  35. M. C. De Sanctis *et al.*, Characteristics of organic matter on Ceres from VIR/Dawn high spatial resolution spectra. *Mon. Not. R. Astron. Soc.* **482**, 2407–2421 (2019). doi: [10.1093/mnras/sty2772](https://doi.org/10.1093/mnras/sty2772)
  36. M. C. De Sanctis *et al.*, Localized aliphatic organic material on the surface of Ceres. *Science* **355**, 719–722 (2017). doi: [10.1126/science.aaj2305](https://doi.org/10.1126/science.aaj2305); pmid: [28209893](https://pubmed.ncbi.nlm.nih.gov/28209893/)
  37. S. Marchi *et al.*, An aqueously altered carbon-rich Ceres. *Nat. Astron.* **3**, 140–145 (2019). doi: [10.1038/s41550-018-0656-0](https://doi.org/10.1038/s41550-018-0656-0)
  38. A. R. Hendrix, F. Vilas, J.-Y. Li, Ceres: Sulfur deposits and graphitized carbon. *Geophys. Res. Lett.* **43**, 8920–8927 (2016). doi: [10.1002/2016GL070240](https://doi.org/10.1002/2016GL070240)
  39. B. E. Clark, B. Hapke, C. Pieters, D. Britt, “Asteroid space weathering and regolith evolution” in *Asteroids III*, W. F. Bottke Jr., A. Cellino, P. Paolicchi, R. P. Binzel, Eds. (Univ. of Arizona Press, 2002), pp. 585–599.
  40. R. Brunetto, M. J. Loeffler, D. Nesvorný, S. Sasaki, G. Strazzulla, “Asteroid surface alteration by space weathering processes” in *Asteroids IV*, P. Michel, F. E. DeMeo, W. F. Bottke, Eds. (Univ. of Arizona Press, 2015), pp. 597–616.
  41. C. M. Pieters, S. K. Noble, Space weathering on airless bodies. *J. Geophys. Res. Planets* **121**, 1865–1884 (2016). doi: [10.1002/2016JE005128](https://doi.org/10.1002/2016JE005128); pmid: [29862145](https://pubmed.ncbi.nlm.nih.gov/29862145/)
  42. D. N. DellaGiustina *et al.*, Exogenic basalt on asteroid (101955) Bennu. *Nat. Astron.* **10.1038/s41550-020-1195-z** (2020). doi: [10.1038/s41550-020-1195-z](https://doi.org/10.1038/s41550-020-1195-z)
  43. F. J. Ciesla, S. A. Sandford, Organic synthesis via irradiation and warming of ice grains in the solar nebula. *Science* **336**, 452–454 (2012). doi: [10.1126/science.1217291](https://doi.org/10.1126/science.1217291); pmid: [22461502](https://pubmed.ncbi.nlm.nih.gov/22461502/)
  44. J. L. Molaro, S. Byrne, J.-L. Le, Thermally induced stresses in boulders on airless body surfaces, and implications for rock breakdown. *Icarus* **294**, 247–261 (2017). doi: [10.1016/j.icarus.2017.03.008](https://doi.org/10.1016/j.icarus.2017.03.008)
  45. J. L. Molaro *et al.*, In situ evidence of thermally induced rock breakdown widespread on Bennu’s surface. *Nat. Commun.* **11**, 2913 (2020). doi: [10.1038/s41467-020-16528-7](https://doi.org/10.1038/s41467-020-16528-7); pmid: [32518333](https://pubmed.ncbi.nlm.nih.gov/32518333/)
  46. D. S. Lauretta *et al.*, Episodes of particle ejection from the surface of the active asteroid (101955) Bennu. *Science* **366**, eaay3544 (2019). doi: [10.1126/science.aay3544](https://doi.org/10.1126/science.aay3544); pmid: [31806784](https://pubmed.ncbi.nlm.nih.gov/31806784/)
  47. A. A. Simon *et al.*, In-flight calibration and performance of the OSIRIS-REx Visible and IR Spectrometer (OVIRS). *Remote Sens.* **10**, 1486 (2018). doi: [10.3390/rs10091486](https://doi.org/10.3390/rs10091486)
  48. P. R. Christensen, E. Engle, S. Anwar, S. Dickenshied, D. Noss, N. Gorelick, M. Weiss-Malik, “JMARS – A Planetary GIS,” American Geophysical Union Fall Meeting, San Francisco, CA, 14 to 18 December 2009; <https://ui.adsabs.harvard.edu/abs/2009AGUFMIN22A.06C.abstract>.
  49. D. C. Reuter, A. A. Simon, A. Lunsford, D. S. Lauretta, Origins, Spectral Interpretation, Resource Identification, Security, Regolith Explorer (OSIRIS-REx): Visible and InfraRed Spectrometer (OVIRS) Bundle. NASA Planetary Data System (2019); <https://sbn.psi.edu/pds/resource/orex/ovirs.html>.

## ACKNOWLEDGMENTS

We are grateful to the entire OSIRIS-REx Team for making the encounter with Bennu possible and to C. W. V. Wolner for editorial review. We thank the developers of the JMARS open source software ([https://jmars.mars.asu.edu/open\\_source](https://jmars.mars.asu.edu/open_source)) for assistance with Bennu-specific visualization (48). **Funding:** A.A.S., H.H.K., V.E.H., D.S.L., H.C., J.P.E., D.C.R., D.N.D., S.A.S., D.R.G., L.F.L., A.R., and C.A.B. were supported by NASA under contract NNM10AA11C issued through the New Frontiers Program. B.R. acknowledges funding support from the Royal Astronomical Society (RAS) and the UK Science and Technology Facilities Council (STFC). **Author contributions:** Investigation: A.A.S., D.S.L., D.C.R., V.E.H., and H.H.K. Data validation: A.A.S., D.C.R., V.E.H., and D.R.G. Data curation: A.A.S., D.C.R., H.H.K., V.E.H., D.R.G., D.N.D., and C.A.B. Conceptualization: A.A.S., D.S.L., D.C.R., V.E.H., H.H.K., J.P.E., A.R., B.R., M.A.B., L.F.L., and S.A.S. Methodology: A.A.S., D.S.L., D.C.R., V.E.H., H.H.K., J.P.E., B.R., M.A.B., L.F.L., and S.A.S. Formal analysis: A.A.S., H.H.K., and V.E.H. Writing or editing: A.A.S., H.H.K., V.E.H., D.S.L., H.C., J.P.E., D.C.R., D.N.D., S.A.S., D.R.G., L.F.L., A.R., B.R., M.A.B., and C.A.B. **Competing interests:** We declare no competing interests. **Data and materials availability:** All OVIRS spectral data from the Detailed Survey and Reconnaissance phases are available via the Planetary Data System at <https://sbn.psi.edu/pds/resource/orex/ovirs.html> (49). Full resolution maps and corresponding 1 $\sigma$  uncertainty maps are available in FITS format as data S1 to S6.

## SUPPLEMENTARY MATERIALS

[science.sciencemag.org/content/370/6517/eabc3522/suppl/DC1](https://science.sciencemag.org/content/370/6517/eabc3522/suppl/DC1)  
Materials and Methods  
Supplementary Text  
Figs. S1 to S6  
References (50–52)  
Data S1 to S6

20 April 2020; accepted 27 August 2020  
Published online 8 October 2020  
[10.1126/science.abc3522](https://doi.org/10.1126/science.abc3522)

## Widespread carbon-bearing materials on near-Earth asteroid (101955) Benu

Amy A. Simon, Hannah H. Kaplan, Victoria E. Hamilton, Dante S. Lauretta, Humberto Campins, Joshua P. Emery, M. Antonietta Barucci, Daniella N. DellaGiustina, Dennis C. Reuter, Scott A. Sandford, Dathon R. Golish, Lucy F. Lim, Andrew Ryan, Benjamin Rozitis and Carina A. Bennett

*Science* **370** (6517), eabc3522.

DOI: 10.1126/science.abc3522 originally published online October 8, 2020

### The complex history of Benu's surface

The near-Earth asteroid (101955) Benu is a carbon-rich body with a rubble pile structure, formed from debris ejected by an impact on a larger parent asteroid. The Origins, Spectral Interpretation, Resource Identification, Security, Regolith Explorer (OSIRIS-REx) spacecraft is designed to collect a sample of Benu's surface and return it to Earth. After arriving at Benu, OSIRIS-REx performed a detailed survey of the asteroid and reconnaissance of potential sites for sample collection. Three papers present results from those mission phases. DellaGiustina *et al.* mapped the optical color and albedo of Benu's surface and established how they relate to boulders and impact craters, finding complex evolution caused by space weathering processes. Simon *et al.* analyzed near-infrared spectra, finding evidence for organic and carbonate materials that are widely distributed across the surface but are most concentrated on individual boulders. Kaplan *et al.* examined more detailed data collected on the primary sample site, called Nightingale. They identified bright veins with a distinct infrared spectrum in some boulders, which they interpreted as being carbonates formed by aqueous alteration on the parent asteroid. Together, these results constrain Benu's evolution and provide context for the sample collected in October 2020.

*Science*, this issue p. eabc3660, p. eabc3522, p. eabc3557

#### ARTICLE TOOLS

<http://science.sciencemag.org/content/370/6517/eabc3522>

#### SUPPLEMENTARY MATERIALS

<http://science.sciencemag.org/content/suppl/2020/10/07/science.abc3522.DC1>

#### RELATED CONTENT

<http://science.sciencemag.org/content/sci/370/6513/158.full>  
<http://science.sciencemag.org/content/sci/370/6517/672.full>  
<http://science.sciencemag.org/content/sci/370/6517/eabc3660.full>  
<http://science.sciencemag.org/content/sci/370/6517/eabc3557.full>  
<http://advances.sciencemag.org/content/advances/6/41/eabc3350.full>  
<http://advances.sciencemag.org/content/advances/6/41/eabd3649.full>  
<http://advances.sciencemag.org/content/advances/6/41/eabc3699.full>

#### REFERENCES

This article cites 48 articles, 8 of which you can access for free  
<http://science.sciencemag.org/content/370/6517/eabc3522#BIBL>

Use of this article is subject to the [Terms of Service](#)

---

*Science* (print ISSN 0036-8075; online ISSN 1095-9203) is published by the American Association for the Advancement of Science, 1200 New York Avenue NW, Washington, DC 20005. The title *Science* is a registered trademark of AAAS.

Copyright © 2020 The Authors, some rights reserved; exclusive licensee American Association for the Advancement of Science. No claim to original U.S. Government Works

PERMISSIONS

<http://www.sciencemag.org/help/reprints-and-permissions>

Use of this article is subject to the [Terms of Service](#)

---

*Science* (print ISSN 0036-8075; online ISSN 1095-9203) is published by the American Association for the Advancement of Science, 1200 New York Avenue NW, Washington, DC 20005. The title *Science* is a registered trademark of AAAS.

Copyright © 2020 The Authors, some rights reserved; exclusive licensee American Association for the Advancement of Science. No claim to original U.S. Government Works